International Journal of Reliability, Risk and Safety: Theory and Application

Online ISSN: 2676-3346

Vol. 7/ Issue 2/ Year 2024/ pp. 52-61
DOI: 10.22034/IJRRS.2024.7.2.5
Received: 06 September 2024, Revised: 03 November 2024, Accepted: 05 November 2024
Available online at: https://www.ijrrs.com

Original Research Article

Health Monitoring Algorithm for Turbofan Engine Using Cascade Feedforward Neural Networks

Mostafa Mahmoudi, Mostafa Khazaee*, Sanaz Ghezeljeh, Seyyed Mohammad Mirmohamadi, and Mehdi Jahromi

Aerospace Faculty, Malek-Ashtar University of Technology, Tehran, Iran

*** khazaee_m@mut.ac.ir**

Abstract

Today, health monitoring systems for turbine engines have become a vital requirement in the aviation industry. In this paper, different fault detection methods of turbine engines are reviewed based on previous research to reveal the importance of the problem and existing challenges. The existing methods use the engine signals for diagnostics, which are heavily affected by operating conditions and disturbances. The faults effect on the performance charts of the F100-PW-220 engine is detected by neural network technique to alleviate the signal variation problem. Some common faults in this type of engine are modeled, including compressor fouling, turbine blade corrosion, and fuel injection problems. The proposed method is effective in a wide range of engine working conditions such as first moments of take-off with afterburner, take-off at 0.1 M, subsonic cruise flight at 0.8 M without afterburner in 10000, 20000, and 40000 feet altitude, supersonic cruise flight at 1.6 M with afterburner in the same altitudes. The cascade neural network with probabilistic transfer functions is used in this paper and shows satisfactory fault detection, while the required training dataset is much less than the previous works. This method facilitates the fast implementation of the system due to the small training dataset and improves the diagnostics accuracy over operational time.

Keywords: Cascade Neural Network; EHMS; Fault detection; Health monitoring; Turbine engine.

Nomenclature

CFNN	Cascade Feedforward Neural Network
EHMS	Engine Health Monitoring System
FD	Fault Detection
(H)LPC	(High) Low Pressure Compressor
(H)LPT	(High) Low-Pressure Turbine

1. Introduction

The aircraft turbine engine consists of many complex components and subsystems that are working together. A fault in one of these components can engage the other subsystems and result in subsequent performance degradation and possible loss of propulsion.

The propulsion in aircraft is the most important system, and many operation abortions, accidents, and crashes are related to the malfunctions in engines. Maintenance costs in the lifecycle of air vehicles are higher than the purchase price. In addition, the costs and downtimes of unscheduled repairs are higher than those of the scheduled ones. Thus, the performance monitoring of engines has emerged to increase the safety level and reliability [1]. The failure of different engine stages results in reliability degradation due to the interaction of these coupled systems [2].

The aircraft engine control and health monitoring system (EHMS), performance monitoring system, and structural health monitoring are developed to cope with this problem [2] and [3]. EHMS provides many advantages for aircraft operators, such as cost reduction, hazardous mission prevention, fuel efficiency, increased safety level, and lower maintenance costs compared to traditional troubleshooting approaches [4].

1.1 Literature Review

The researchers utilized different methods for engine performance monitoring. In the late 1960s, Urban

How to cite this article:
M. Mahmoudi, M. Khazaee, S. Ghezeljeh, S.M. Mirmohamadi, and M. Jahromi, "Health monitoring algorithm for turbofan engine using cascade feedforward neural networks," *International Journal of Reliability, Risk and Safety: Theory and Application*, vol. 7, no. 2, pp. 52-61, 2024, doi: 10.22034/IJRRS.2024.7.2.5.

introduced the gas path analysis method [5], which made significant progress in gas turbine fault detection. The initial applications of expert systems started in 1980, and they remain and are developing as one of the best tools for turbine diagnostics [6]. The gas path analysis is a linear method introduced by urban and subsequent derivatives, which are proposed based on optimal estimation [7]. Stamatis et al. consider the nonlinear behavior of the engine, a method based on nonlinear models and traditional optimization for the first time [8].

Dietz et al. propose the neural network (NN) for gas turbine fault detection for the first time [9]. NNs are used frequently due to the data-driven development that can be obtained from experimental tests and fast fault detection time after training. Fuster et al. utilize the fuzzy rule-based expert system for engine fault diagnostics [6]. Li studies the technological advancement of fault detection based on gas turbine performance analysis, such as data validation and error identification [10]. The main methods for fault diagnostics use linear models, nonlinear models, neural networks, genetic algorithms, expert systems, fuzzy logic, and transient measurement techniques.

Verma et al. propose an algorithm with an assumption on the variation of input parameters WF, N1, N2, and EGT to diagnose faults in HPC, LPC, HPT, LPT, and fan using fuzzy rules [11]. NASA conducts a major research program on performance health monitoring of gas turbines through measurement of the main fluctuation [12]. Demirci et al. developed the Automatic Engine Health Monitoring System (AEHMS) based on a fuzzy inference system [1]. Ebrahimi and Mollazade investigate the intelligent method for EHMS reactor engine faults that uses oscillation signals and an adaptive neural-fuzzy inference system [13]. Farsi develops a convolutional neural network (CNN) based on the experimental vibration data recorded from a bearing fault setup. The proposed CNN determines the location and size of the damage with high accuracy [15]. Abdul-Aziz et al. develop an engine monitoring approach based on the semi-experimental equations [14].

Mohamadi et al. present a new technology for technical faults of gas turbine engines using a dynamic neural network [15]. Pinelli et al. introduce engine health monitoring through gas path analysis (GPA), which relies on field measurements [16]. Puggina and Venturini research different elements and approaches for diagnostic and prognostic systems [17]. The advantages are components' costs, scheduled repair activities, and optimization of spare parts for efficient maintenance and performance improvement of gas turbines.

Tahan et al. thoroughly review and evaluate the engine performance monitoring detection techniques and their evolution over time [18]. They consider the performance diagnostic methods first and then the techniques for high-quality data generation, which are based on engine model fidelity and intelligent computation algorithms. The predictive maintenance decision-making structure in accordance with the identified disruption in the engine performance is studied.

Adamowicz and Żywica concentrate on the Brayton thermodynamic cycle in which a radial or centrifugal compressor delivers the air to add fuel to the combustion chamber. The power turbine drives the shaft using the expanding combustion products. The faults are considered as the variation of process efficiency [19]. Jianzhong et al. emphasize the importance of prognostics and health management in commercial airplanes. Due to the limitations of the sensors in the old aircraft, one of the key challenges for EHMS is to find the appropriate health index with sufficient correlation with real failure [20].

Balakrishnan et al. analyze thirteen engine parameters from different flight conditions with an aircraft EHMS based on a whale optimization algorithm and artificial neural network technique. The metrics are accuracy, error, and false alarms for comparison with other methods [21]. Szrama combines NN pattern recognition and automated feature engineering to make a turbofan engine monitoring algorithm [22]. Due to the use of diverse predictors in NN, the accuracy of this method compared with machine learning is satisfactory, and it has lower processing costs.

Aditya et al. try to go beyond the physical model of the engine for condition monitoring and life extension, using CFM 56 engine characteristic parameters, e.g., margins of the surge and EGT, to train the deep learning models for diagnostics [23]. The dataset is augmented with simulation in some steady-state cruise flight conditions. In addition, degradation is considered by variations in the fan's mass flow capacity and efficiency. Thakkar and Chaoui study engine degradation as the fault to be diagnosed. The remaining useful life is estimated through a deep-layer recurrent NN model for dynamic maintenance planning with an extensive semi-experimental dataset [24].

Some challenges in the previous works slowed down the adoption of EHMS despite their achievement. The main problem is that the training dataset is not available for many aircraft turbofan engines due to limited sensors and variations in flight routes and conditions. Thus, the aircraft owners and airlines could not afford the initial costs to make the required dataset. To cope with this problem, the present paper is devoted to developing a fault detection algorithm that does not require much training data and has a simple and fast structure.

The next section addresses the engine fault modeling to make the simulated dataset. Section 4 introduces the fault detection method based on a cascade feedforward neural network. The results are presented in section 5, which discusses the results. The last section concludes the research with respect to the defined contribution.

2. Engine Fault Modeling

The engine modeling is conducted using comprehensive thermodynamic software that covers the design and off-

design points. The following faults are modeled in this paper to be used for diagnostics.

2.1 Compressor fouling

The fouling is the adhesion of air impurities to the surface of compressor blades, which results in a change in the entrance angle, airfoil form, and roughness. This is the most frequent reason for compressor failure and causes 75 to 85% performance reduction in turbine engines. Fortunately, this fault can be reduced with the cleansing of depositions to fix the gas path near the initial form.

Figure 1. Salt fouling on the compressor blades at 18000 working hours [25]

Figure 1 shows a sample of the compressor in which the blades are affected by fouling with salt spot marking. These fouling are removable and more probable on the outer sides of the blade. The modeling of fouling in the present research is considered for low-pressure compressor blades, as depicted in Table 1 for different levels of fault.

Table 1. Values for modeling of compressor fouling

Fault intensity	Delta isentropic efficiency	Delta flow capacity
Very Low Fouling	-0.5	-1
Low Fouling	-1	-2
Medium Fouling	-1.5	-3
High Fouling	-2	-4
Very High Fouling	-2.5	-5

Based on these values, the compressor fouling is done per [26] through the isentropic efficiency and flow capacity. To consider this fault in the off-design points of the F100-PW-220 engine model, the parameters variation are from -5 to 0% on flow capacity and -2.5 to 0% on isentropic efficiency for different flight conditions.

2.2 Fault in the fuel system

The interruption in the fuel system is another frequent fault that is modeled based on Table 2 [26]. The fuel interruption could not be modeled with an isentropic efficiency drop, which is not available at the off-design points. Thus, the input parameters should be used to change this parameter to reflect the fault. The pressure ratio of the combustion chamber is one of the parameters that directly affect isentropic efficiency, EGT, and thrust. So, this parameter is used to model the fuel faults.

Table 2. Values for modeling of fuel system malfunctions

Fault intensity	Delta Burner P/P %
Very Low malfunction of fuel delivery system	2
Low malfunction of fuel delivery system	3
Medium malfunction of fuel delivery system	4
High malfunction of fuel delivery system	5
Very High malfunction of fuel delivery system	6

2.3 Turbine blade erosion

The erosion is the material removal of flow components by abrasive particles such as sand, fly ash, and water. Balan and Tabakoff explain how erosion reduces the performance due to surface roughness increase, tip clearance increase, leading-edge breakage, trailing edge thickness reduction, and shortened blade chords [27]. Hamed et al. investigate the major reasons that affect turbine erosion, including particle properties, gas flow path, blade geometry, operational conditions, and blade material [28].

In the turbine section, the effect of the abrasive particles, which enter with fuel products, is more severe, as shown in Figure 2. If the cooling holes are blocked or destructed, excessive heating, failure, and creep of the blade will occur. Industrial filters can eliminate a major portion of particles, while aircraft engines are susceptible to them [29].

Figure 2. Erosion of turbine blades [29]

Table 3 shows the modeling parameters for erosion fault in high-pressure turbine blades in five levels of occurrence.

Table 3. Values for modeling of turbine blade erosion

Fault intensity	Delta isentropic efficiency (%)	Delta flow capacity (%)
Very Low Erosion	-0.5	1
Low Erosion	-1	2
Medium Erosion	-1.5	3
High Erosion	-2	4
Very High Erosion	-2.5	5

To model the turbine erosion, two effective parameters, i.e., isentropic efficiency and flow capacity, are changed for the off-design points of the F100-PW-220 engine. The variations in the flow capacity are 0 to 5%, and the isentropic efficiency is from -2.5 to 0% for eight different flight phases, as shown below.

- Take-off @ Mach 0 with afterburner on
- Take-off @ Mach 0.1 with afterburner on
- Subsonic cruise @ M 0.8 without afterburner in 10000, 20000, 40000 feet altitude
- Supersonic cruise @ M 1.6 with afterburner in 10000, 20000, 40000 feet altitude

2.4 Turbine engine model and data

In the real case, all parameters of the engine could not be measured. Therefore, the required parameters should be derived from the model per available sensors on the mentioned turbofan engine, as shown in Table 4.

Table 4. Available sensors on turbofan engines [30]

Parameter	Measurement description
N l	Speed of low-pressure shaft
N2	Speed of low-pressure shaft
PO	Environment pressure
PS13	Bypass static pressure
P2	Fan inlet pressure
P2S	High-pressure compressor (HPC) inlet pressure
PS3	Outlet static pressure of HPC
P41	Inlet pressure of high-pressure turbine (HPT)
P4S	Inlet pressure of low-pressure turbine (LPT)
PS	Outlet pressure of LPT
TO	Ambient temperature
Tl 2	Fan inlet temperature
T13	Bypass outlet temperature
T2S	HPC inlet temperature
T3	HPC outlet temperature
T41	HPT inlet temperature
T4S	LPT inlet temperature
TS	LPT outlet temperature
WF	Fuel flow rate
W2S	HPC inlet flow rate
W3	HPC outlet flow rate
W41	HPT inlet flow rate
W4S	LPT inlet flow rate
W2	Fan inlet flow rate
WS	LPT outlet flow rate

The engine performance is modeled as a twin-spool low bypass ratio engine per the following assumptions. The sections and calculation points are shown in Figure 3.

- The environment condition for the design point is SLS (seal level static).
- The performance variables, such as efficiencies and pressure loss, are constant, i.e., constant polytrophic efficiency is assumed for the fan, compressor, and turbine.
- The cooling flows' percent are constant.
- The nozzle is converging for subsonic flight and converging-diverging for supersonic regimes.
- The thrust analysis is done with active and inactive afterburners.

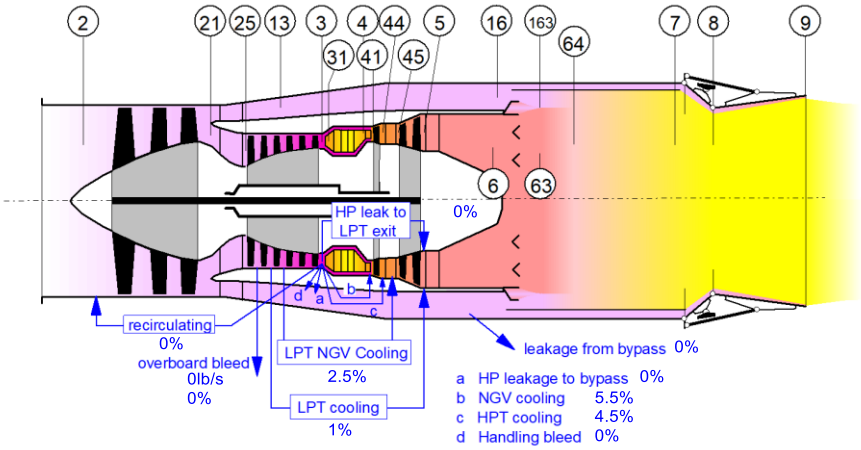

Figure 3. Thermodynamic model of twin-spool turbofan engine with mixing flow

The available specifications from the F100-PW-220 verify the model, and some of the engine characteristics maps are shown as follows, e.g., the thrust-SFC map in Figure 4 for different bypass ratios and range of afterburner temperatures.

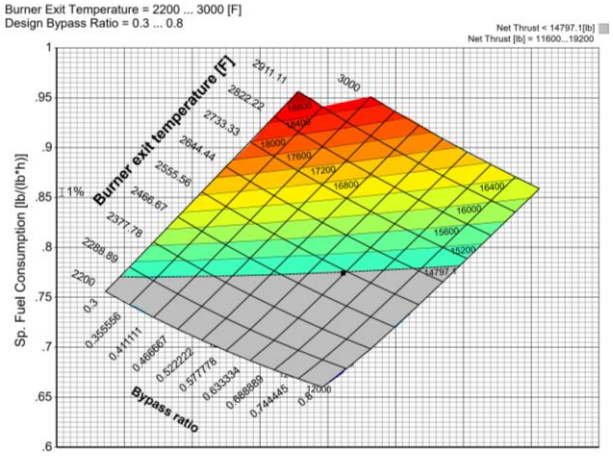

Figure 4. Thrust and specific fuel consumption vs. bypass ratio and afterburner temperature

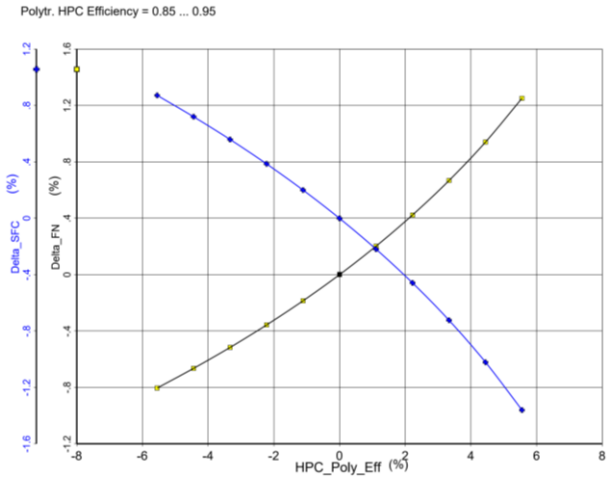

Figure 5. Thrust and SFC sensitivity analysis to polytrophic efficiency on and specific fuel consumption vs bypass ratio and afterburner temperature

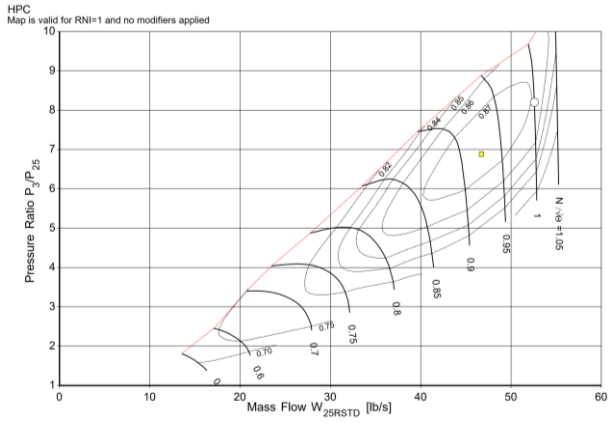

Figure 6. Thrust, SFC, HPT, and isentropic efficiency sensitivity analysis to HPT tip clearance

The faults are modeled, as mentioned in Section 3, through variations on the relevant performance characteristics or geometric parameters. The variations are incorporated in the model with a similar method for sensitivity analysis, as depicted in Figures 5 and 6.

3. Fault Detection Algorithm

The cascade forward neural network (CFNN) is used to develop the turbofan engine fault detection algorithm. In this type of network model, the input and output are connected through indirect relations. The hidden layers are nonlinear, with an activation function that can be combined with perceptron networks. This network structure includes the direct and indirect connections from input to output. The governing equations of CFNN can be written as below.

$$y = \sum_{i=1}^{n} f^i \omega_i^i x_i + f^o \left(\sum_{j=1}^{k} \omega_j^o f_j^h \left(\sum_{i=1}^{n} \omega_{ji}^h x_i \right) \right) \quad (1)$$

where f^i is the activation function between the input and output layers and ω_i^i is the weight of this connection. If any bias is added to the input and the activation function of each neuron is in the hidden layer f^h, the above equation becomes as follows.

$$y = \sum_{i=1}^{n} f^i \omega_i^i x_i + f^o \left(\omega^b + \sum_{j=1}^{k} \omega_j^o f^h \left(\omega_j^b + \sum_{i=1}^{n} \omega_{ji}^h x_i \right) \right) \quad (2)$$

In this research, CFNN is trained on the simulation dataset for the mentioned turbofan engine. Therefore, the neurons of the input layer $x_{t-1}, \ldots, x_{t-p}$ are the obtained characteristics from the engine models in different healthy conditions. The CFNN model architecture is shown in Figure 7 for the identification of one condition.

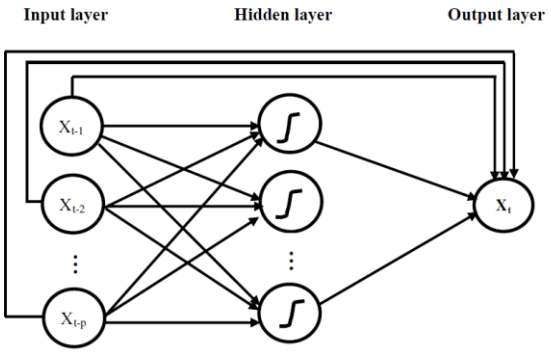

Figure 7. CFNN model architecture for prediction of time-series

The direct relation between input and output is clear in Figure 7, which needs the network weight to be estimated, and the neurons of the input layer increase the number of characteristics for identification. Similar to Feedforward NN, the back-propagation algorithm in CFNN consists of three steps.

- Input feedforward pattern
- Error counting
- Weight tuning

Assuming that ω is a weight vector with a length of s, which belongs to a set of network weights with cost function $e = \frac{1}{2}(X_t - \hat{X}_t)$. It is assumed that Q is a $n \times n$ positive symmetric matrix. Then, the conjugate gradient

optimization algorithm can be applied as follows with an initial $Q^{(0)}$. The initial weight gradient is calculated as below.

$$g^{(o)} = \frac{\partial e}{\partial \omega^{(0)}} = \frac{\partial e}{\partial \omega}|_{\omega=\omega^{(0)}} = \left[\frac{\partial e}{\partial \omega_1{}^{(0)}} \cdots \frac{\partial e}{\partial \omega_s{}^{(0)}}\right]^T \quad (3)$$

If $g^{(o)} = 0$, then the process will be terminated, and the optimal weight is obtained. Else, the process will continue with $d^{(o)} = g^{(o)}$.

4. Results of the FD Algorithm

4.1 Dataset Description

The dataset for the healthy or faulty engine in different flight regimes is simulated using the thermodynamic model per section 3 for the F100-PW-220 turbofan engine. The database is briefly described in Appendix A.

4.2 Fault Detection Results

The proposed algorithm is implemented as a cascade feedforward neural network with three layers in the first and second layers; the radbas transform function or probabilistic is used along with the softmax transform function in the output layer. This network is very fast and accurate for the three mentioned faults, but it needs much less data. This model, which requires only 20% of the whole dataset, is shown in Figure 8.

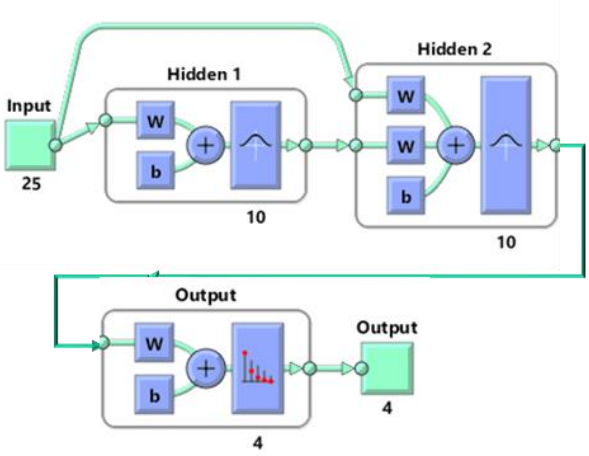

Figure 8. Proposed CFNN model structure for EHMS

The performance graph demonstrates the trend of cross-energy variation in the training, validation, and test processes, as shown in Figure 9. The best validation performance is achieved at epoch 89.

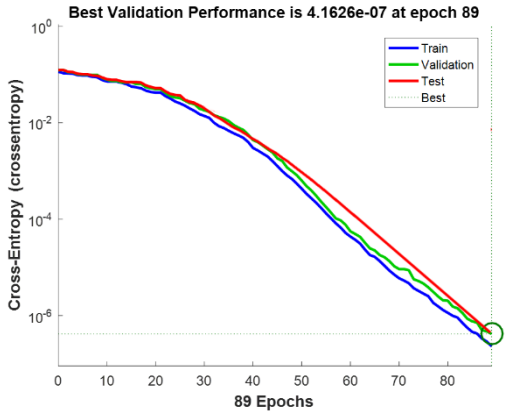

Figure 9. Performance graph of CFNN training, validation, and testing on the F100-PW-220 simulated dataset

Table 5 explains the cells of the confusion matrix for engine fault detection. This matrix demonstrates the capability and validity of the NN in the detection of different conditions of the system. The values in diagonal cells are the number of correct detections for each fault. The last cell is the overall detection accuracy. The off-diagonal cells represent the incorrect detection of faults. The definition of each cell based on the considered faults in section 3 for aircraft turbine engines is clarified in the following table.

Table 5. Definition of a confusion matrix for engine fault detection

H*	H classified as TE	H classified as CF	H classified as IB	H accuracy
TE is classified as H	TE+	TE classified as CF	TE is classified as IB	TE accuracy
CF is classified as H	CF is classified as TE	CF†	CF is classified as IB	CF accuracy
IB is classified as H	IB is classified as TE	IB is classified as CF	IB‡	IB accuracy
H sensitivity	TE sensitivity	CF sensitivity	IB sensitivity	Detection Accuracy

* H: Healthy condition.
\+ TE: Turbine erosion
† CF: Compressor fouling
‡ IB: Injector blocking

The last row shows the sensitivity of the classifier with respect to each fault. The last column shows the detection accuracy for each healthy or faulty condition, which gives the confidence of the classifier for each class.

The accuracy of the proposed FD algorithm is tested, as shown in Figure 10. The achieved accuracy is satisfactory with respect to the accuracy of the simulated dataset, but there is just one incorrect classification.

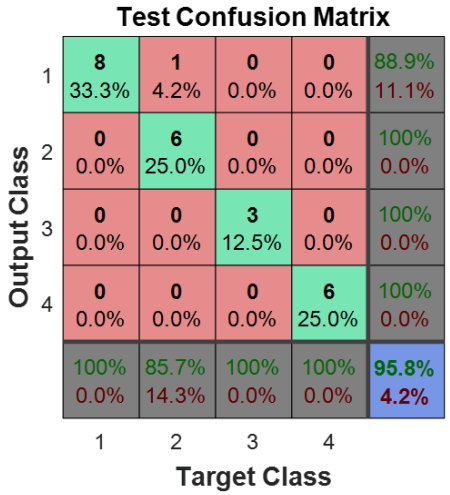

Figure 10. Confusion matrix of the proposed algorithm on test dataset

As it can be perceived from the confusion matrix on all datasets in Figure 11, the acceptable fault detection accuracy of the algorithm is training with less data (20% instead of 70%), validation, and testing is evaluated at 99.4%.

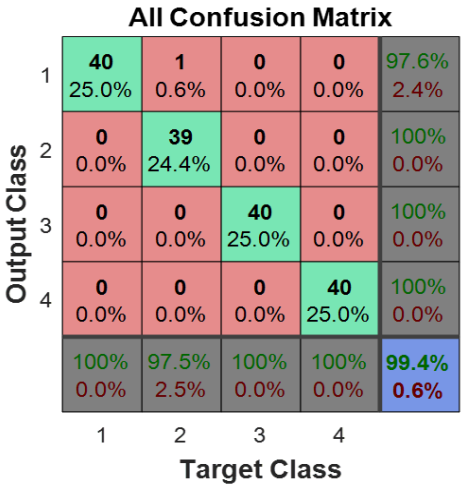

Figure 11. Confusion matrix of the proposed algorithm on all dataset

5. Conclusion

The literature review determines that the main goals were finding the proper fault detection and remaining useful life of components through diagnostic methods, modeling, data analysis, and identification techniques. The main challenges are the lack of hazardous, expensive flight tests and effective performance characteristics. Therefore, first, the simulation and diagnostics methods should be selected and verified, and then the dependency on the accuracy should be reduced to the amount of training data.

This paper makes a simulated dataset at 160 points for three frequent faults (compressor fouling, turbine erosion, injector blockage) with five severity levels in turbofan engines in different flight conditions, including takeoff, subsonic, and supersonic cruise.

The 25 mentioned parameters are directly measurable in most turbofan engines and registered in the dataset. The variation of these parameters has been studied, but it is not enough for training. The cascade networks are used because the input vector is fed in two steps and increases the hidden layer weights to fit on system behavior. This architecture helps to handle the different clusters of data for healthy and faulty conditions over various flight conditions.

Future works based on the achievement of this paper will focus on reducing the required data for machine learning algorithms and robustness to data loss, trend, bias, and noise that are inevitable in aircraft engines.

Conflict of Interests

No conflict of interest has been expressed by the authors.

6. References

[1] S. Demirci, C. Hajiyev and A. Schwenke, "Fuzzy logic-based automated engine health monitoring for commercial aircraft," *Aircraft engineering and aerospace technology*, vol. 80, no. 5, pp. 516-525, 2008. doi: https://doi.org/10.1177/1748006X21989661.

[2] M. Nadjafi and P. Gholami, "Bayesian inference of reliability growth-oriented Weibull distribution for multiple mechanical stages systems," *International Journal of Reliability, Risk and Safety: Theory and Application*, vol. 3, no. 1, pp. 77-84, 2020. doi: https://doi.org/10.30699/IJRRS.3.1.9.

[3] D. Culley *et al.*, "More intelligent gas turbine engines," North Atlantic Treaty Organization, France, Rep. AC/323(AVT-128)TP/255, 2009.

[4] R. K. Yedavalli and R. K. Belapurkar, "Application of wireless sensor networks to aircraft control and health management systems," *Control Theory and Applications*, vol. 9, pp. 28-33, 2011. doi: https://doi.org/10.1007/s11768-011-0242-9.

[5] M. M. Bidgoli, M. A. S. Ashtiani and M. Mahmoudi, "Intelligent performance monitoring of aircraft engine using fuzzy logic," in *13th International Conference of Iranian Aerospace Society*, Tehran, Iran, 2014. (in Persian)

[6] L. A. Urban, "Parameter selection for multiple fault diagnostics of gas turbine engines," Journal of Engine Power, vol. 10, no. 7, pp. 225-230, 1975, doi: https://doi.org/10.1115/1.3445969.

[7] P. Fuster, A. Ligeza and A. Martin, "Abductive diagnostic procedure based on an and/or/not graphs for expected behaviour: Application to gas turbine," in 10th International Congress and Exhibition on Condition Monitoring and Diagnostic Engineering Management, Espoo, Finland, 1997, pp. 511-520.

[8] L. A. Urban, *Gas turbine engine parameter interrelationships*, 2nd ed. Pennsylvania: Hamilton Standard Division of United Aircraft Corporation, 1969.

[9] A. Stamatis, K. Mathioudakis, M. Smith and K. Papailiou, "Gas turbine component fault identification by means of adaptive performance modeling," American Society of Mechanical Engineers, vol. 79085, pp. 90-GT-376, 1990. https://doi.org/10.1115/90-GT-376.

[10] W. E. Dietz, E. I. Kiech and M. Ali, "Jet and rocket engine fault diagnosis in real time," *Journal of Neural Network Computation*, vol. 1, no. 1, pp. 5-18, 1989.

[11] Y. G. Li, "A gas turbine diagnostic approach with transient measurements," *Proceedings of the Institution of Mechanical Engineers, Part A: Journal of Power and Energy*, vol. 217, no. 2, pp. 169-177, 2003, doi: https://doi.org/10.1243/09576500360611317.

[12] R. Verma, N. Roy and R. Ganguli, "Gas turbine diagnostics using a soft computing approach," *Applied mathematics and computation*, vol. 172, no. 2, pp. 1342-1363, 2006, doi: https://doi.org/10.1016/j.amc.2005.02.057.

[13] S. S. Wang, W. M. Wang, Y. Q. Shi and Y. Zhang, "Gas turbine condition monitoring and prognosis: A review," *Advanced Engineering Forum*, vol. 2, pp. 694-699, 2011. doi: https://doi.org/10.4028/www.scientific.net/AEF.2-3.694.

[14] E. Ebrahimi and K. Mollazade, "Intelligent fault classification of a tractor starter motor using vibration monitoring and adaptive neuro-fuzzy inference system," *Insight-non-destructive Testing and Condition Monitoring*, vol. 52, no. 10, pp. 561-566, 2010, doi: https://doi.org/10.1784/insi.2010.52.10.561.

[15] M. A. Farsi, "Identification of size and location of bearing damage via deep learning," *International Journal of Reliability, Risk, and Safety: Theory and Application*, vol. 4, no. 1, pp. 69-74, 2021, doi: https://doi.org/10.30699/IJRRS.4.1.9.

[16] A. Abdul-aziz, M. R. Woike, J. D. Lekki and G. Y. Baaklini, "Health monitoring of a rotating disk using a combined analytical-experimental approach," National Aeronautics and Space Administration, Ohio, USA, Rep. 2009-215675, 2009.

[17] R. Mohammadi, E. Naderi, K. Khorasani and S. Hashtrudi-Zad, "Fault diagnosis of gas turbine engines by using dynamic neural networks," in *IEEE International Conference on Quality and Reliability (ICQR)*, 2010, pp. 365-376, doi: https://doi.org/10.1115/GT2010-23586.

[18] M. Pinelli, P. R. Spina and M. Venturini, "Gas turbine health state determination: Methodology approach and field application," *International Journal of Rotating Machinery*, vol. 2012, no. 1, p. 2012, Art. no. 142173, doi: https://doi.org/10.1155/2012/142173.

[19] N. Puggina and M. Venturini, "Development of a statistical methodology for gas turbine prognostics," *Journal of Engine Gas Turbine Power*, vol. 134, no. 2, 2012, Art. no. 022401, doi: https://doi.org/10.1115/1.4004185.

[20] M. Tahan, E. Tsoutsanis, M. Muhammad and Z. A. Karim, "Performance-based health monitoring, diagnostics and prognostics for condition-based maintenance of gas turbines: A review," *Applied Energy*, vol. 198, pp. 122-44, 2017, doi: https://doi.org/10.1016/j.apenergy.2017.04.048.

[21] M. Adamowicz and G. Żywica, "Advanced gas turbines health monitoring systems," *Diagnostyka*, vol. 19, no. 2, pp. 77-87, 2018, doi: http://dx.doi.org/10.29354/diag/89730.

[22] S. Jianzhong, L. Chaoyi, L. Cui, G. Ziwei and W. Rong, "A data-driven health indicator extraction method for aircraft air conditioning system health monitoring," *Chinese Journal of Aeronautics*, vol. 32, no. 2, pp. 409-416, 2019, doi: https://doi.org/10.1016/j.cja.2018.03.024.

[23] N. Balakrishnan, A. I. Devasigamani, K. R. Anupama and N. Sharma, "Aero-engine health monitoring with real flight data using whale optimization algorithm based artificial neural network technique," *Optical Memory and Neural Networks*, vol. 30, pp. 80-96, 2021, doi: https://doi.org/10.3103/S1060992X21010094.

[24] S. Szrama, "Turbofan engine health status prediction with neural network pattern recognition and automated feature engineering," *Aircraft Engineering and Aerospace Technology*, vol. 96, no. 11, pp. 19-26, 2024, doi: https://doi.org/10.1108/AEAT-04-2024-0111.

[25] A. Aditya, T. Nikolaidis, A. C. Manuel and S. Togni, "Implementation of Artificial Intelligence for Aircraft Engine Health Monitoring and Prognostics," in *ASME Turbo Expo 2024: Turbomachinery Technical Conference and Exposition*. *Volume 4: Controls, Diagnostics, and Instrumentation*, London, United Kingdom, 2024, doi: https://doi.org/10.1115/GT2024-127081.

[26] U. Thakkar and H. Chaoui, "Prognostic and health management of an aircraft turbofan engine using machine learning," in *IEEE Vehicle Power and Propulsion Conference*, Milan, Italy, 2023, doi: https://doi.org/10.1109/VPPC60535.2023.10403231.

[27] R. Kurz and K. Brun, "Fouling mechanisms in axial compressors," *Journal of Engineering for Gas Turbines and Power*, vol. 134, 2012, Art. no. 032401, doi: https://doi.org/10.1115/1.4004403.

[28] A. D. Fentaye and K. G. Kyprianidis, "An intelligent data filtering and fault detection method for gas turbine engines," in *MATEC Web Conference*, Vol. 314, 2020, Paper 02007, doi: https://doi.org/10.1051/matecconf/202031402007.

[29] C. Balan and W. Tabakoff, "A method of predicting the performance deterioration of a compressor-cascade due to sand erosion," in 21st Aerospace Sciences Meeting, Nevada, USA, 1983, doi: https://doi.org/10.2514/6.1983-178.

[30] A. A. Hamed, W. Tabakoff and R. Wenglarz, "Erosion, deposition, and their effect on performance," in *Turbine Aerodynamics, Heat Transfer, Materials, and Mechanics*, T. I-P. Shih and V. Yang, Ed. Place of publication: American Institute of Aeronautics and

Astronautics (AIAA), 2014, pp. 585-611, doi: https://doi.org/10.2514/5.9781624102660.0585.0612.
[31] R. Kurz and K. Brun, "Degradation in gas turbine systems," *Journal of Engine Gas Turbine Power*, vol. 123, no. 1, pp. 70-77, 2001, doi: https://doi.org/10.1115/1.1340629.
[32] T. S. Sowers, G. Kopasakis and D. L. Simon, "Application of the systematic sensor selection strategy for turbofan engine diagnostics," in Turbo Expo: Power for Land, Sea, and Air, 2008. https://doi.org/10.1115/GT2008-50525.
[33] A. D. Fentaye and K. G. Kyprianidis, "An intelligent data filtering and fault detection method for gas turbine engines," in *MATEC Web Conference*, Vol. 314, 2020, Paper 02007, doi: https://doi.org/10.1051/matecconf/202031402007.
[34] C. B. Meher-Homji and R. Bhargarva, "Condition monitoring and diagnostic aspects of gas turbine transient response," *International Journal of Turbo and Jet Engines*, vol. 11, no. 1, pp. 99-111, 1994, doi: https://doi.org/10.1515/TJJ.1994.11.1.99.
[35] T. Kobayashi and D. L. Simon, "A hybrid neural network-genetic algorithm technique for aircraft engine performance diagnostics," *Journal of Propulsion and Power*, vol. 21, no. 4, pp. 751-758, 2005, doi: https://doi.org/10.2514/1.9881.
[36] A. Algarni, M. Tozan and A. Jamal, "Failure forecasting of aircraft air conditioning/cooling pack with field data," *Journal of Aircraft*, vol. 44, no. 3, pp. 996-1002, 2012, doi: https://doi.org/10.2514/1.26561.
[37] J. Hare, S. Gupta, N. Najjar, P. D'Orlando and R. Walthall, "System-level fault diagnosis with application to the environmental control system of an aircraft," in *SAE 2015 AeroTech Congress and Exhibition*, 2015, Paper 2015-01-2583, doi: https://doi.org/10.4271/2015-01-2583.
[38] A. Silva, N. Najjar, S. Gupta and P. D'Orlando, "Wavelet-based fouling diagnosis of the heat exchanger in the aircraft environmental control system," in *SAE 2015 AeroTech Congress and Exhibition*, 2015, Paper 2015-01-2582, 2015, doi: https://doi.org/10.4271/2015-01-2582.
[39] N. Najjar, J. Hare, P. D'Orlando, G. Leaper, K. Pattipati, A. Silva, S. Gupta and R. Walthall, "Heat exchanger fouling diagnosis for an aircraft air-conditioning system," in *SAE 2013 AeroTech Congress and Exhibition*, 2013, Paper 2013-01-2250, doi: https://doi.org/10.4271/2013-01-2250.
[40] J. Ma, C. Lu and H. Liu, "Fault diagnosis for the heat exchanger of the aircraft environmental control system based on the strong tracking filter," *PloS One*, vol. 10, no. 3, 2015, Art. no. e0122829, doi: https://doi.org/10.1371/journal.pone.0122829.

Appendix

The simulation results extensively cover different operational conditions, and two examples of on-design and off-design points are shown in Figures A1 and A2.

Appendix A. Database introduction

The engine dataset for fault detection is made using the simulations of the prescribed performance model and fault models in section 3. The fault severity is considered at five levels for the compressor fouling, fuel injection, and turbine blade erosion. In addition to faulty conditions, the healthy engine is simulated on design and off-design points to cover the effect of variations due to flight and environmental conditions. The performance data for the combination of health/faults is derived in eight different flight phases, as shown below.

- Take-off @ Mach 0 with afterburner on
- Take-off @ Mach 0.1 with afterburner on
- Subsonic cruise @ M 0.8 without afterburner in 10000, 20000, 40000 feet altitude
- Supersonic cruise @ M 1.6 with afterburner in 10000, 20000, 40000 feet altitude

The simulation contains many parameters (183 values) which are not available for measurement on the real engine. Thus, the parameters which are measurable and can be estimated directly are used as the input of fault detection algorithm per Table 4. Among these parameters, 25 parameters and their deviations from healthy condition are selected based on sensitivity analysis and used for training of fault detection model.

```
          W         T         P        WRstd      Reheat on
Station  lb/s       F        psia       lb/s      FN       =  24888.87 lb
 amb               59.00    14.696
  1    224.999     59.00    14.696                 TSFC     =    2.0512 lb/(lb*h)
  2    224.999     59.00    14.696   225.000       WF Burner=   3.18696 lb/s
 13     86.963    284.06    44.793    34.165       s NOX    =    0.8468
 21    138.036    284.06    44.793    54.230       BPR      =    0.6300
 25    138.036    284.06    44.345    54.778       Core Eff =    0.4594
  3    133.205    951.48   363.630     8.880       Prop Eff =    0.0000
 31    119.401    951.48   363.630                  P3/P2    =   24.744
  4    122.588   2550.00   349.085    12.432
 40    128.800   2479.70   349.085                  NGV      2 Stage HPT
 41    130.180   2464.94   349.085    13.014       P16/P6   =   0.79278
 43    130.180   1882.46   116.605                 A63      =    262.13 in²
 44    136.392   1843.04   116.605                 A163     =    937.87 in²
 45    139.843   1808.47   115.439    37.228       A64      =   1200.00 in²
 49    139.843   1505.15    58.267                 XM63     =   0.60469
  5    141.223   1494.29    58.267    69.134       XM163    =   0.05782
  6    141.223   1494.29    55.936                 XM64     =   0.17482
 16     86.963    284.06    44.345                 P63/P6   =   0.97000
 64    219.490   1090.76    46.667                 P163/P16 =   0.97000
  7    104.546   3500.00    44.819                 WF total =  14.18129 lb/s
  8    239.180   3404.35    44.819   214.055       A8       =    665.10 in²
Bleed    0.000    284.06    44.345                 CD8      =   0.97444
-----------------------------------------------    Ang8     =     12.78 °
Efficiencies:   isentr  polytr    RNI    P/P       P8/Pamb  =   3.04978
 Outer LPC      0.8602  0.8800  1.000  3.048       WLkBy/W25=   0.00000
 Inner LPC      0.8602  0.8800  1.000  3.048       WCHN/W25 =   0.05500
 HP Compressor  0.8692  0.9000  1.964  8.200       WCHR/W25 =   0.04500
 Burner         0.9970                 0.960       Loading  =    100.00 %
 HP Turbine     0.9019  0.8900  3.150  2.994       WCLN/W25 =   0.02500
 LP Turbine     0.8978  0.8900  1.395  1.981       WCLR/W25 =   0.01000
 Mixer          1.0000                             WBHD/W21 =   0.00000
 Reheat         0.9200                 0.960       WF Reheat=  10.99433 lb/s
                                                   XM7      =   0.32987
-----------------------------------------------    far7     =   0.06556
HP Spool mech Eff 0.9900  Nom Spd  13450 rpm       WBLD/W25 =   0.00000
LP Spool mech Eff 0.9900  Nom Spd  10400 rpm       PWX      =     400.0 hp
-----------------------------------------------    P16/P13  =    0.9900
P2/P1= 1.0000 P25/P21=0.9900 P45/P44= 0.9900       P6/P5    =    0.9600
Con-Di Nozzle:                                     A9/A8    =   1.62000
 A9*(Ps9-Pamb)     177.698                         CFGid    =   0.92050
-----------------------------------------------
hum [%]     war0       FHV     Fuel
   0.0   0.00000   18638.0    Generic
```

Figure A1. Engine simulation on-design point with active afterburner

```
mixed Turbofan
Alt=40000ft / Mn=2.000 ISA ,  Rel GG Speed=1.000


          W         T         P        WRstd      Reheat on
Station  lb/s       F        psia       lb/s      FN       =  19163.04 lb
 amb               -69.70     2.720
  1    200.400    242.12    21.298                 TSFC     =    2.2555 lb/(lb*h)
  2    200.400    242.12    21.298   160.848       WF Burner=   2.44608 lb/s
 13     93.881    424.84    44.102    40.853       s NOX    =    1.2413
 21    106.519    424.84    44.102    46.352       BPR      =    0.8814
 25    106.518    424.84    43.753    46.722       Core Eff =    0.6258
  3    102.790   1111.77   301.013     8.735       Prop Eff =    0.5810
 31     92.138   1111.77   301.013                  P3/P2    =    14.133
  4     94.585   2669.52   288.357    11.841       P5/P2    =    2.3536 EPR
 40     99.378   2600.86   288.357                  NGV      2 Stage HPT
 41    100.443   2586.34   288.357    12.406       P16/P6   =   0.89647
 43    100.443   1977.31    94.844                 A63      =    290.10 in²
 44    105.236   1940.66    94.844                 A163     =    909.90 in²
 45    107.899   1907.04    93.895    36.077       A64      =   1200.00 in²
 49    107.899   1621.84    50.127                 XM63     =   0.45845
  5    108.965   1611.21    50.127    63.838       XM163    =   0.07321
  6    108.965   1611.21    48.432                 XM64     =   0.16709
 16     93.881    424.84    43.418                 P63/P6   =   0.97498
 64    193.458   1122.27    43.414                 P163/P16 =   0.95293
  7     92.087   3500.00    41.910                 WF total =  12.00627 lb/s
  8    212.406   3387.57    41.910   202.889       A8       =    630.53 in²
Bleed    0.000    424.84    43.753                 CD8      =   0.97353
-----------------------------------------------    Ang8     =     13.23 °
Efficiencies:   isentr  polytr    RNI    P/P       P8/Pamb  =  15.40800
 Outer LPC      0.8737  0.8857  1.011  2.071       WLkBy/W25=   0.00000
 Inner LPC      0.8737  0.8857  1.011  2.071       WCHN/W25 =   0.05500
 HP Compressor  0.8763  0.9029  1.576  6.880       WCHR/W25 =   0.04500
 Burner         0.9974                 0.958       Loading  =    91.41 %
 HP Turbine     0.8983  0.8859  2.483  3.040       WCLN/W25 =   0.02500
 LP Turbine     0.8811  0.8731  1.081  1.873       WCLR/W25 =   0.01000
 Mixer          1.0000                             WBHD/W21 =   0.00000
 Reheat         0.9215                 0.965       WF Reheat=   9.56019 lb/s
                                                   XM7      =   0.30825
-----------------------------------------------    far7     =   0.06286
HP Spool mech Eff 0.9900  Speed    13450 rpm       WBLD/W25 =   0.00000
LP Spool mech Eff 0.9900  Speed     8849 rpm       PWX      =     400.0 hp
-----------------------------------------------    P16/P13  =    0.9845
P2/P1= 1.0000 P25/P21=0.9921 P45/P44= 0.9900       P6/P5    =    0.9662
Con-Di Nozzle:                                     A9/A8    =   1.62000
 A9*(Ps9-Pamb)    3891.665                         CFGid    =   0.90124
-----------------------------------------------
hum [%]     war0       FHV     Fuel
   0.0   0.00000   18638.0    JP-4
```

Figure A2. Engine simulation off-design point at 40,000 feet and Mach 2 with active afterburner